JOURNAL OF GEOPHYSICAL RESEARCH, VOL. 116, F04013, doi:10.1029/2011JF002019, 2011

Calculations of in-snow NO_2 and OH radical photochemical production and photolysis rates: A field and radiative-transfer study of the optical properties of Arctic (Ny-Ålesund, Svalbard) snow

J. L. France,[1] M. D. King,[1] J. Lee-Taylor,[2] H. J. Beine,[3] A. Ianniello,[4] F. Domine,[5] and A. MacArthur[6]

Received 4 March 2011; revised 11 August 2011; accepted 17 August 2011; published 1 November 2011.

[1] Depth-integrated production rates of OH radicals and NO_2 molecules from snowpacks in Ny-Ålesund, Svalbard, are calculated from fieldwork investigating the light penetration depth (*e*-folding depth) and nadir reflectivity of snowpacks during the unusually warm spring of 2006. Light penetration depths of 8.1, 11.3, 5.1, and 8.2 cm were measured for fresh, old, marine-influenced, and glacial snowpacks, respectively (wavelength 400 nm). Radiative-transfer calculations of the light penetration depths with reflectivity measurements produced scattering cross sections of 5.3, 9.5, 20, and 25.5 $m^2\ kg^{-1}$ and absorption cross sections of 7.7, 1.4, 3.4, and 0.5 $cm^2\ kg^{-1}$ for the fresh, old, marine-influenced, and glacial snowpacks, respectively (wavelength 400 nm). Photolysis rate coefficients, *J*, are presented as a function of snow depth and solar zenith angle for the four snowpacks for the photolysis of H_2O_2 and NO_3^-. Depth-integrated production rates of hydroxyl radicals are 1270, 2130, 950, and 1850 nmol $m^{-2}\ h^{-1}$ (solar zenith angle of 60°) for fresh, old, marine-influenced, and glacial snowpacks, respectively. Depth-integrated production rates of NO_2 are 32, 56, 11, and 22 nmol $m^{-2}\ h^{-1}$ (solar zenith angle of 60°) for the fresh, old, marine-influenced, and glacial snowpacks, respectively. The uncertainty of repeated light penetration depth measurement was determined to be ~20%, which propagates into a 20% error in depth-integrated production rates. A very simple steady state hydroxyl radical calculation demonstrates that a pseudo first-order loss rate of OH radicals of $\sim 10^2$–$10^4\ s^{-1}$ is required in snowpack. The snowpacks around Ny-Ålesund are thick enough to be considered optically infinite.

Citation: France, J. L., M. D. King, J. Lee-Taylor, H. J. Beine, A. Ianniello, F. Domine, and A. MacArthur (2011), Calculations of in-snow NO_2 and OH radical photochemical production and photolysis rates: A field and radiative-transfer study of the optical properties of Arctic (Ny-Ålesund, Svalbard) snow, *J. Geophys. Res.*, *116*, F04013, doi:10.1029/2011JF002019.

1. Introduction

[2] In polar regions, the oxidative capacity of the lower atmosphere (e.g., the sum of ozone, HO_x radicals and hydrogen peroxide) is greater than predicted by conventional atmospheric chemistry models [e.g., *Dibb et al.*, 2004; *Domine and Shepson*, 2002; *Jones and Wolff*, 2003; *Mauldin et al.*, 2001; *Yang et al.*, 2002] and photochemistry in the underlying snowpack has been implicated. Fluxes of NO, NO_2 and HONO from the snowpack to the atmospheric boundary layer have been observed during many field campaigns and have been shown to have a snowpack photochemical source [*Beine et al.*, 2001, 2002, 2003, 2008; *Dibb et al.*, 2004; *Grannas et al.*, 2007; *Honrath et al.*, 1999, 2000b, 2002; *Jones et al.*, 2000, 2001; *Wang et al.*, 2008]. Laboratory and modeling studies have demonstrated that the source of NO_2 is the photolysis of nitrate anion [*Anastasio and Chu*, 2009; *Boxe and Saiz-Lopez*, 2008; *Chu and Anastasio*, 2003; *Cotter et al.*, 2003; *Couch et al.*, 2000; *Dubowski et al.*, 2001, 2002; *Honrath et al.*, 2000a]:

$$NO_3^- + h\nu \rightarrow NO_2 + O^-. \quad (1)$$

The oxygen radical anion produced in reaction (1) can react with water to generate the highly reactive OH radical [e.g., *Mack and Bolton*, 1999]:

$$O^- + H_2O \rightarrow OH + OH^-. \quad (2)$$

[1]Department of Earth Sciences, Royal Holloway University of London, Egham, UK.
[2]Atmospheric Chemistry Division, National Center for Atmospheric Research, Boulder, Colorado, USA.
[3]Air Quality Research Centre, University of California, Davis, California, USA.
[4]Consiglio Nazionale delle Ricerche-IIA, Monterotondo Scalo, Italy.
[5]Laboratoire de Glaciologie et Géophysique de l'Environnement, CNRS, St. Martin D'Heres, France.
[6]Grant Institute, University of Edinburgh, Edinburgh, UK.

0148-0227/11/2011JF002019

Hydroxyl (OH) radicals are also produced in the snowpack through the photolysis of hydrogen peroxide:

$$H_2O_2 + h\nu \rightarrow 2OH. \quad (3)$$

The production of OH radicals, in the presence of O_2, within the snowpack creates a reactive oxidizing medium. Hydroxyl radicals are implicated in the photolytic production of acetaldehyde, formaldehyde and oxygenated organic fluxes observed from snowpacks [*Anastasio et al.*, 2007; *Couch et al.*, 2000; *Dassau et al.*, 2002; *Grannas et al.*, 2004, 2007; *Hutterli et al.*, 2003, 2004; *Jacobi et al.*, 2004; *Shepson et al.*, 1996; *Wang et al.*, 2008]. Measured photoformation rates of OH radicals in snow at Summit, Greenland suggest that the photolysis of hydrogen peroxide and, to a lesser extent, nitrate, are the predominant sources of OH radicals [*Anastasio et al.*, 2007; *France et al.*, 2007]. Hydrogen peroxide photolysis has been shown to produce 93%–99% of the total OH radicals produced in snowpack from nitrate and hydrogen peroxide photolysis [*Chu and Anastasio*, 2005]. The importance of OH radicals for snow chemistry has been recently demonstrated through chemical box modeling [*Bock and Jacobi*, 2010].

[3] Hydroxyl radicals may also play an important role in the production of halogens and halogen oxides from snowpack [*Abbatt et al.*, 2010]. In situ bromine oxidation by OH radicals in sea salt particles and from frozen halide nitrate solutions has been demonstrated in the laboratory [*Abbatt et al.*, 2010; *George and Anastasio*, 2007; *Matthew et al.*, 2003]. It is speculated that similar reactions may be important in the release of reactive halogens from snowpack [*George and Anastasio*, 2007]. Recent one-dimensional modeling work has demonstrated that bromine recycling on snow from deposited bromine to gas phase bromine is sufficient to deplete tropospheric ozone to a few nmol mol^{-1} in the boundary layer [*Piot and von Glasow*, 2008].

[4] The depth-integrated photochemical production rate, F, of NO_2 and OH radicals is calculated using the photolysis rate coefficient, J, for reactions (1) and (3) within the snowpack and the concentration of the reactive chromophore in the snowpack, i.e., $[NO_3^-]$ and $[H_2O_2]$. The photolysis rate coefficient, J, depends on the photon flux within the snow (spherical irradiance, i.e., what many authors loosely term "actinic flux"), the quantum yield of the photolytic reaction (i.e., reaction (1) or (3)) and the absorption cross section of the chromophore. The spherical irradiance within the snowpack at any depth can be calculated using the coupled snow-atmosphere radiative-transfer model TUV-snow [*Lee-Taylor and Madronich*, 2002]. The optical properties of snowpacks in this model can be described by a scattering and an absorption cross section, derived from measurements of the snowpack surface reflectance and e-folding depth of the snowpack.

[5] The e-folding depth is a measure of the light penetration in optically thick snowpacks. A few centimeters into a thick snowpack the light within the snowpack is effectively diffuse and isotropic owing to multiple scattering [*Warren*, 1982]. The irradiance of light within the snow below the first few centimeters has been demonstrated to decay exponentially with depth [*Fisher et al.*, 2005; *King and Simpson*, 2001]. The e-folding depth, ε, is the depth of snowpack required to reduce the irradiance to $1/e$ (~37%) of its initial value:

$$\frac{I_z}{I_{z'}} = e^{-\frac{z-z'}{\varepsilon}}, \quad (4)$$

where I_z is the irradiance intensity at a depth z within the snowpack, z' is an initial depth into the snowpack, z is a deeper depth than z' and ε is the asymptotic e-folding depth.

[6] When comparing e-folding depths from different studies, different authors often compare the liquid equivalent e-folding depth, which is the e-folding depth normalized for the snow density [*King and Simpson*, 2001]:

$$\varepsilon_{liq} = \frac{\rho_{snow}}{\rho_{water}} \times \varepsilon, \quad (5)$$

where ε_{liq} is the liquid equivalent e-folding depth, ρ_{snow} is the density of snow, and ρ_{water} is the density of water. Unless explicitly stated, all e-folding depths quoted in this paper are for snow depth and are not normalized to liquid equivalent.

[7] The authors have previously studied snowpack absorption and scattering properties of Arctic, Antarctic and midlatitude mountainous snowpacks [*Beine et al.*, 2006; *Fisher et al.*, 2005; *King and Simpson*, 2001]. The study presented here measures the snowpack optical properties and can be used to estimate potential chemical snow-air fluxes at Ny-Ålesund, an important high-latitude, marine-influenced, atmospheric chemistry, field site which has hosted numerous air-snow NO_x exchange studies [e.g., *Amoroso et al.*, 2006; *Beine et al.*, 1997, 2003].

[8] *Wiscombe and Warren* [1980] demonstrated that for thin, shallow snowpacks, the ground layer under the snowpack can lower the snow surface albedo in the UV visible. In thin snowpacks the ground under the snow may absorb photons and thus reduce photolytic reaction rates in the snow, relative to a thick snowpack. At previous study sites, the snowpack has been thick enough to be considered optically semi-infinite [e.g., *Beine et al.*, 2006; *Fisher et al.*, 2005; *France et al.*, 2011]. The Ny-Ålesund field sites had areas of thin snow cover (less than 40 cm deep), and this study considers the effect of snowpack thickness on snowpack photolytic production rates.

[9] The aims of this study were to (1) measure the snowpack optical and physical properties in the vicinity of Ny-Ålesund, Svalbard through measurement of snowpack stratigraphy, surface light reflectance and light penetration depth; (2) determine in-snow photochemical production rates of OH radical and NO_2 molecules owing to the photolysis of H_2O_2 and NO_3^-; (3) assess the uncertainty of replicate field measurements of e-folding depth; (4) investigate the depth required for optically semi-infinite snowpack, with a real snowpack; and (5) estimate the order of magnitude of a pseudo first-order loss rate of hydroxyl radicals in the snowpack.

2. Optical Fieldwork Measurements

[10] Many exploratory snow pits (>50) were dug at various locations around Ny-Ålesund, Svalbard (78°55′N, 11°56′E) in early April 2006. Seven of these snow pits were studied

in detail: Two marine-influenced snowpacks (within 50 m of the sea), three snow pits near the Italian station in Ny-Ålesund town, and two snow pits in nearby glacial accumulation zones, Comfortless and Brøggerhalvøya glaciers. At each site, a snow pit approximately 2 m long by 1 m wide by 1 m deep was dug in an east–west direction, ensuring the area surrounding the snow pit was as undisturbed as possible. At each site measurements of *e*-folding depth, surface reflectance, stratigraphy and chemical measurements were performed. The chemical measurements determined major soluble anion and cation concentrations in melted snow samples.

2.1. Measuring *e*-Folding Depths (Light-Penetration Depths)

[11] Solar irradiance penetrating the snowpack was measured using a spectrometer with the solar radiation guided through a fiber optic. A multimode silica fiber-optic was glued into a 50 cm length of 6.35 mm diameter stainless steel tubing, with a PTFE cosine corrector as a robust entrance optic. The fiber optic probe has been demonstrated during previous experiments [*Beine et al.*, 2006; *Fisher et al.*, 2005; *France et al.*, 2010b; *King and Simpson*, 2001; *King et al.*, 2005]. The probe was connected to a USB powered S2000 Ocean Optics spectrometer with a potential wavelength range from 320 nm to 700 nm (1 in 400 signal-to-noise ratio). The fiber optic probe was inserted ~50 cm horizontally into the fresh, vertical south wall (north facing) of the snow pit as close to the surface as possible without causing disturbance to the snow surface (~5 cm depth). For each snow depth, up to three spectra were recorded and this process was repeated at ~3 cm depth intervals deeper into the snowpack until the signal-to-noise ratio became detrimental (~5), typically at (or before) a snowpack depth of 20 cm. Spectra were also measured at each depth with longer integration periods to saturate the CCD of the spectrometer at visible wavelengths in order to obtain a reasonable UV signal. The PTFE tip of the fiber optic was laterally offset by 5–10 cm to minimize the damage caused to the snowpack under study. The lateral offset was achieved by inserting the fiber optic probe vertically below a previous measurement and reducing or increasing the angle (maximum ~10°) the fiber optic probe makes with the snowpack wall in the horizontal plane. The fiber optic is directed into the snowpack horizontally and approximately parallel to the snowpack surface, so the PTFE tip does not face upward or downward with depth into the snowpack. The direction faced by the PTFE tip does not affect the irradiance measured as the light within the snowpack is isotropic below the first few centimeters [*Warren*, 1982]. The fiber optic probes are inserted horizontally into the snowpack with the aid of a sprit level to ensure that the depth of the irradiance sensor is accurately known.

[12] The snow pits were not back-filled during the irradiance measurements. The fiber optic probe measures irradiance horizontally into the snowpack, at least 49 cm away from the pit wall. Diffuse light entering the snowpack through the snow pit is 3–6 *e*-folding depths further away from the probe than the light from the surface. Therefore, it can be estimated that at the deepest depths, light from the snowpack wall will contribute 0.2%–5% of light measured by the probe, but typically less than 1% of light propagating from above the fiber optic probes. Back filling the snow pit with excavated material will not reproduce the original snowpack radiance field, and covering the snow pit may be detrimental to the radiance field within the snowpack.

[13] Spectra were field calibrated for wavelength using a mercury discharge lamp, and dark electrical noise on the CCD was removed by subtracting a dark spectrum recorded in the field at the same temperatures as the field measurements. Ambient chilling of the spectrometers resulted in significant dark noise reduction.

[14] At the same time as each in-snow irradiance measurement, an atmospheric downwelling spectral irradiance from 350 nm to 1050 nm was recorded using a GER1500 spectroradiometer, with a cosine corrector, mounted on a tripod, 1.5 m above the snow surface, next to the snow pit. These measurements of downwelling solar irradiance allow for changing downwelling irradiance owing to changing overhead sky conditions. No in-snow irradiance measurements were made during rapidly changing sky conditions, and when possible measurements were recorded under overcast sky (diffuse) conditions or measurements were made around solar noon to minimize any solar zenith angle change.

[15] Solar irradiances within the snowpack were measured from 320 nm to 700 nm. Solar radiances reflected from the snowpack were measured from 350 nm to 1050 nm. There is limited evidence of scattered light within the GER1500 spectroradiometer affecting the radiance values between 350 nm and 380 nm, thus a lower limit of 400 nm was imposed on the reflectivity data. Radiative-transfer calculations of light propagation in the snowpack require reflectivity and in-snow irradiances measured for each wavelength. Thus optical scattering and absorption coefficients are reported for wavelengths of 400–700 nm.

[16] For each measurement of in-snow irradiance, I_z^{snow}, a concurrent downwelling atmospheric solar irradiance was measured, I_z^{sky}, the subscript z on the downwelling solar irradiance measurement represents the depth of the measurement of irradiance in the snowpack which it was concurrent with. The ratios of the in-snow to surface downwelling irradiances, i.e., $I_z^{\mathrm{snow}}/I_z^{\mathrm{sky}}$, were fitted to equation (6) for every wavelength (400 nm to 700 nm) to determine the wavelength dependant *e*-folding depths, ε, for each snowpack:

$$\frac{I_z^{\mathrm{snow}}}{I_z^{\mathrm{sky}}} = \frac{I_{z'}^{\mathrm{snow}}}{I_{z'}^{\mathrm{sky}}} e^{\left(\frac{-(z-z')}{\varepsilon}\right)}, \tag{6}$$

where z is the depth in the snowpack and z' is a reference depth.

[17] The method used to calculate *e*-folding depth does not require an absolute intensity calibration of the spectrometers. To estimate the repeatability of the *e*-folding depth measurement, an analysis of multiple *e*-folding depth measurements of the same snowpack was undertaken. To our knowledge this has not previously been performed. A visually homogeneous snowpack was chosen, which was a large drift behind a shipping container and with large (50 cm) thick uniform layers of snow. At this site, 7 separate *e*-folding depth measurements were recorded within the same snow pit face, approximately 1 m apart. In-snow irradiance was

measured at 4 different depths at each of the 7 positions. Only four depths were used for each *e*-folding measurement as the experiments were time consuming. Determination of *e*-folding depth in other snow pits typically used 6–10 measurement depths of in-snow irradiance. The experiment is designed to assess the uncertainty in replicate *e*-folding depth measurements and the natural variability of snow cover. The uncertainty in repeat *e*-folding depth measurements and a measure of the natural variability of snow cover cannot be separated in the experiment described.

2.2. Measuring Snowpack Surface Reflectance

[18] Snowpack surface reflectance was measured with the dual spectroradiometer (nadir reflectance) method using two GER1500 spectroradiometers [*Duggin and Philipson*, 1982]. One spectroradiometer measured the upwelling radiance of the snow surface, and the second spectroradiometer measured the upwelling radiance of a white spectralon plate of known reflectivity under exactly the same sky conditions. A cross-calibration of the spectroradiometers was performed by simultaneously measuring reflectivity of the same spectralon plate with both spectroradiometers. The work described here represents an improvement on previous studies by using a dual beam method to measure snowpack reflectivity. The signal-to-noise ratio in the resultant reflectance measurements is significantly higher (typically double) than the single beam method previously used [*Beine et al.*, 2006; *Fisher et al.*, 2005]. At each snowpack site snowpack reflectance was measured over a transect of 5–10 points about 5–15 cm apart, with 10 measurements averaged at each point. Typically 10–20 cross-calibration measurements were performed between the spectrometers. The calibration and maintenance of the spectroradiometers and spectralon panels is undertaken by the NERC Field Spectroscopy Facility. The uncertainty of the reflectance measurements due to natural surface variation and measurement error is ~5% [*France*, 2008].

2.3. Physical Snowpack Measurements

[19] In addition to the optical measurements, the snowpack stratigraphy, temperature and density were recorded. The temperature was recorded at 10 cm depth intervals using a NIST traceable thermocouple. Density was measured using a 200 cm^3 snow block cutter at 8 cm intervals, and the blocks were weighed in the field. The stratigraphy was recorded using the notation of *Fierz et al.* [2009]. From previous field campaigns, the errors on the snow density measurements have been shown to be ±10% [*Fisher et al.*, 2005]. The temperature probe used was accurate to 0.5°C. A detailed stratigraphy of the snowpack was not recorded as the individual irradiance measurements were spaced at vertical intervals of ~3 cm and the radiative-transfer calculation assumes a homogeneous snowpack.

2.4. Snowpack Chemistry Measurements

[20] Triplicate snow samples were taken in polyethylene centrifuge tubes that were thoroughly rinsed with ultrapure water. The tube was opened and inserted horizontally in the vertical snow pit face, using common precautions to avoid contamination (disposable gloves, facing the wind, etc.). The tubes were stored in a freezer until analysis by ion chromatography, always within 48 h of sampling. Hydrogen peroxide was not measured so concentrations of H_2O_2 are assumed to be 4 μmol l^{-1} from a previous consideration of Arctic snowpack H_2O_2 measurements [*France et al.*, 2010a]. The hydrogen peroxide concentration assumption is justified in the discussion section 5.2. Nitrate concentrations in snow were measured by ion chromatography.

3. Modeling Procedure

[21] A radiative-transfer modeling procedure was used to calculate snowpack-specific cross sections for absorption due to impurities, σ^+_{abs}, and scattering, σ_{scatt}, from the measured snowpack surface reflectance and *e*-folding depths [*Lee-Taylor and Madronich*, 2002]. The atmosphere-snow radiative-transfer model, TUV-snow, was then used to calculate irradiances and photolysis rate coefficients, *J*, in the snowpack to calculate depth-integrated production rates. Depth-integrated production rates may be considered an estimate of the maximum potential flux of photogenerated material from the snowpack to the atmosphere, in the absence of further loss.

3.1. Determination of Snowpack Scattering and Absorption Cross Sections

[22] The optical properties of the Ny-Ålesund snowpacks were modeled with the coupled atmosphere-snow radiative-transfer model, TUV-snow [*Lee-Taylor and Madronich*, 2002], using an eight-stream discrete-ordinates scheme [*Stamnes et al.*, 1988]. TUV-snow has been experimentally validated through comparisons with chemical actinometry in the laboratory [*Phillips and Simpson*, 2005].

[23] A detailed description of the procedure to determine the scattering and absorption coefficients, σ_{scatt} and σ^+_{abs}, respectively, is given by *Lee-Taylor and Madronich* [2002]. The TUV-snow model calculates spherical irradiances within a snowpack with unequally spaced levels, with 1 mm spaced level for the top 0.5 cm and 1 cm spaced levels for the rest of the snowpack. Snowpack thickness is usually set to 1 m, which is optically semi-infinite. The modeled irradiances allow calculation of an *e*-folding depth and snowpack surface reflectance. An *e*-folding depth, ε, is calculated by fitting equation (4) to modeled irradiances at depths, 5, 10, and 15 cm [*Lee-Taylor and Madronich*, 2002]. Snowpack surface reflectance is calculated as the ratio of modeled upwelling and downwelling irradiances at the snow surface.

[24] Albedo and *e*-folding depth were calculated from modeled irradiances for a range of values of scattering and absorption coefficients, σ_{scatt} and σ^+_{abs} These values are interpolated to find combinations of σ_{scatt} and σ^+_{abs} that reproduce the reflectivity or *e*-folding depth measured in the fieldwork. Many combinations of σ_{scatt} and σ^+_{abs} may reproduce snowpack reflectivity or *e*-folding depth, but only one combination of σ_{scatt} and σ^+_{abs} will reproduce both the snowpack reflectivity and the *e*-folding depth. The unique values of σ_{scatt} and σ^+_{abs} that will reproduce both field measured reflectivity and *e*-folding depth are found by plotting the combination of values of σ_{scatt} and σ^+_{abs} that reproduce the reflectivity, and by plotting the combination of values of σ_{scatt} and σ^+_{abs} that reproduce the *e*-folding depth. The intersection of these two plots is the unique

solution of σ_{scatt} and σ^{+}_{abs} that reproduces the field measurements of reflectance and *e*-folding depth. The determination of σ_{scatt} and σ^{+}_{abs} is undertaken by hand, and different users achieve the same result within typically 5%. Values of the scattering and absorption coefficients, σ_{scatt} and σ^{+}_{abs}, are determined in the present study at wavelengths of 400, 425, and 450 nm.

3.2. Fluxes and Depth-Integrated Production Rates

[25] The calculation of depth-integrated production rates (an estimate of the potential molecular flux from the snowpack to the atmosphere assuming no subsequent loss) is briefly outlined below, and a fuller description can be found in the work of *Beine et al.* [2006]. The TUV-snow model is used to calculate photolysis rate constants and spherical irradiances, I, as a function of solar zenith angle, θ, depth, z, and wavelength, λ, using the scattering and absorption coefficients as previously determined for each snowpack. The photolysis rate constant, J, for reaction (1) is calculated according to

$$J(z) = \int_{\lambda_y}^{\lambda_x} \sigma(\lambda, T)\ \Phi(\lambda, T)\ I(\lambda, \theta, z)\ d\lambda, \tag{7}$$

where $\sigma(\lambda, T)$ is the absorption cross section of the chromophore undergoing photolysis (NO_3^- or H_2O_2), $\Phi(\lambda, T)$ is the quantum yield for the photolytic reaction, $I(\lambda, \theta, z)$ is the spherical irradiance, λ is the wavelength, θ is the solar zenith angle, z is the depth, and T is the temperature.

[26] A depth-integrated photolysis rate constant, ν, (or transfer velocity) is calculated according to equation (8) by integrating the photolysis rate constant over the snowpack depth, z:

$$\nu = \int_{z=0\mathrm{m}}^{z=1\mathrm{m}} J(z)\ dz. \tag{8}$$

Finally, the depth integrated production rate of NO_2 or OH is calculated from equation (9) [*Simpson et al.*, 2002]:

$$F = \nu[x]. \tag{9}$$

The concentration, $[x]$, of the chromophore, x, is assumed to be depth independent. The concentration-depth dependence has been shown to be insignificant when determining photochemical fluxes from snowpack, as the concentration-depth dependence of a chromophore tends to decrease over an order of magnitude with snow depth, whereas light irradiance in the snowpack will decrease by many orders of magnitude with snow depth [*France et al.*, 2007, 2010a]. *France et al.* [2007] demonstrated that the depth-integrated production rate of OH radicals from H_2O_2 photolysis changed by ~3%–5% when considering (1) a real concentration depth profile from the South Pole, (2) a depth-independent concentration profile, and (3) a concentration-depth profile based upon an average H_2O_2 concentration over the first two *e*-folding depths. Depth-integrated production rates of OH radicals were calculated using equation (7) for both nitrate and hydrogen peroxide photolysis. A reader who wished to recalculate a depth integrated production rate using their own concentration-depth profiles could use the data provided within Figures 2 and 3 with equation (10) to calculate a new value of F:

$$F = \int_{z=0\mathrm{m}}^{z=1\mathrm{m}} [x]_z\ J\ dz, \tag{10}$$

where $[x]_z$ is the concentration of chromophore at depth z.

[27] The absorption cross section and temperature-dependent quantum yield for reaction (1) were taken from *Chu and Anastasio* [2003]. For reaction (3), the absorption cross section and the temperature-dependent quantum yield were taken from *Chu and Anastasio* [2005]. The absorption cross section for ice was taken from *Warren and Brandt* [2008], with values for wavelengths between 200 nm and 400 nm linearly interpolated where the values are too small to measure.

[28] The calculation of depth-integrated production rates of OH radicals and NO_2 molecules use the latest recommendation of the ice absorption spectrum [*Warren and Brandt*, 2008]. Previously an "ice minimum" absorption spectrum was used, taking the minimum values of ice absorption at each UV-visible wavelength from the work of Perovich, Askebjer and Pope [*Askebjer et al.*, 1997; *Perovich and Govoni*, 1991; *Pope and Fry*, 1997]. The sensitivity of the calculations presented here to the ice absorption spectrum, was checked by calculations of depth-integrated photolysis rate coefficients (transfer velocities) for H_2O_2 photolysis and NO_3^- photolysis for two previously analyzed snowpacks: Cairngorms [*Fisher et al.*, 2005] (a large grained midlatitude snowpack with a large *e*-folding depth) and Alert [*King and Simpson*, 2001] (a cold, small grained snowpack with a small *e*-folding depth). The new ice absorption spectrum makes a small difference to the calculated NO_2 and OH radical depth-integrated photolysis rate coefficients (<0.3%). Thus, previously calculated depth-integrated production rates are not affected by this change to the model. The adoption in the work presented here of the more recent nitrate absorption cross section of *Chu and Anastasio* [2003] as opposed to the nitrate absorption cross section of *Burley and Johnston* [1992] results in a <1% change to depth-integrated photolysis rates, when considering distinctly different snowpacks such as Alert and Cairngorms.

[29] Photolysis rate coefficients were calculated for solar zenith angles from 0° to 90° using clear-sky conditions (no cloud), with no aerosol, an under-snow ground albedo of 0.1, an Earth-Sun distance based upon the day of measurement, daily ozone conditions from the NASA TOMS program [*McPeters et al.*, 1998], longitude, latitude and elevation as shown in Table 1. For Figures 2 and 3 presented later in the paper, an Earth-Sun distance of 10 April 2006 was used.

3.3. Snowpack Thickness

[30] Depth-integrated production rates will typically increase with increasing snowpack depth until the snowpack becomes effectively optically semi-infinite. To explore the effect of snowpack thickness upon snowpack photolysis, two case studies were undertaken. Depth-integrated photolysis rates were calculated for the marine-influenced

Table 1. Measured Environmental Parameters and Derived Absorption (σ^+_{abs}) and Scattering (σ_{scatt}) Coefficients for the Four Characteristic Ny-Ålesund Snowpacks

Snow Description	Snow Temperature (°C)	H_2O_2[a] (μmol L^{-1})	NO_3^-[b] (μmol L^{-1})	*e*-Folding Depth[c] (cm)	Liquid Equivalent *e*-Folding Depth[c] (cm)	σ_{scatt} (m^2 kg^{-1})	σ^+_{abs} (cm^2 kg^{-1})	Latitude (°N)	Longitude (°E)	Elevation (m)	Column Ozone[d] (DU)
Old wind pack	−8	4	2.94	11.3	4.5	9.5	1.4	78.9252	11.9367	~5	421
Marine influenced	−5	4	1.35	5.1	1.9	20	3.4	78.9217	11.9619	~2	421
Fresh wind pack	−3	4	2.53	8.1	3.2	5.3	7.7	78.9252	11.9367	~5	421
Glacial	−4	4	1.24	8.2	2.7	25.5	0.5	78.4525	12.2546	~560	407

[a] H_2O_2 inferred from previous Arctic measurements and not measured during this work.
[b] Concentration is measured in melted snow as mol L^{-1} of water.
[c] Wavelength λ = 400 nm.
[d] Ozone conditions determined from the NASA TOMS program [*McPeters et al.*, 1998].

snowpack (detailed in the section 4) with snowpack thicknesses of 0.1, 0.2, 0.3, 0.4, 0.5, 0.7, and 1 m, each with an under snow albedo of 0.1. The resulting depth-integrated production rate of the snowpack for each thickness was ratioed to the depth-integrated production rate of a semi-infinite snowpack of 1 m thickness. Second, the potential for depth-integrated photolysis rates to be reduced due to measured snow depths in the coastal area of Ny-Ålesund was considered. A 140 m transect of snowpack thickness was measured for the marine-influenced snowpack at Zeppelinhamer (<1 km east of Ny-Ålesund), from the water's edge heading inland, measuring snow thickness at 2 m intervals. For each snowpack thickness, the depth-integrated photolysis rate, $\upsilon(NO_3^-)$, was calculated for a solar zenith angle of 75°.

4. Results

[31] The results are split into three sections: field measurements, the determined optical properties and photolytic calculations. From the seven snow pits investigated in detail, four snowpacks are presented for spring 2006. The snowpacks are described as old wind pack, fresh wind pack, marine influenced, and glacial (accumulation zone). The localities of each of the four snowpacks are shown in Table 1.

4.1. Field Measurements

[32] Measurements of temperature, density, *e*-folding depth, snowpack surface reflectance and snowpack stratigraphy from the four snowpacks are shown in Figure 1. The campaign was typified by an unseasonably warm Winter and Spring for Ny-Ålesund as reported by *Amoroso et al.* [2010]. Consequently, (1) sea ice did not form near Ny-Ålesund, (2) basal ice layers were found in all the near-sea snowpacks, and (3) there were numerous melt-freeze layers [*Amoroso et al.*, 2010]. Thus, the snowpacks measured during this campaign may not be too typical for Ny-Ålesund Spring snowpack.

[33] The *e*-folding depth measurements (Figure 1c) show a peak transmission at a wavelength around 450 nm for the old wind pack, glacial snowpack and marine-influenced snowpack, while the fresh wind pack has a peak transmission at a wavelength of 490 nm. The variation of *e*-folding depth with wavelength is sensitive to small concentrations of light absorbing compounds present in the snowpack [*Warren et al.*, 2006]. The shift in the wavelength of the maximum *e*-folding depth for the fresh windblown snow may be indicative of a snowpack impurity with an absorption in the UV-blue part of the spectrum; a pattern consistent with the absorption spectra of HULIS [*Hoffer et al.*, 2006]. The largest value of *e*-folding depth is for the old wind pack, probably owing to the observed larger grain size of the snow particles [*Fisher et al.*, 2005] relative to the other snowpacks, resulting from snow metamorphism [e.g., *Domine et al.*, 2008]. The smallest *e*-folding depths were found in snowpacks that had been heavily marine influenced. The marine-influenced snowpack has a small *e*-folding depth and a curious feature centered at 550 nm in its wavelength dependant reflectance (Figure 1b). Both these features may be attributed to different scattering properties of the marine-influenced snowpack compared to the other three

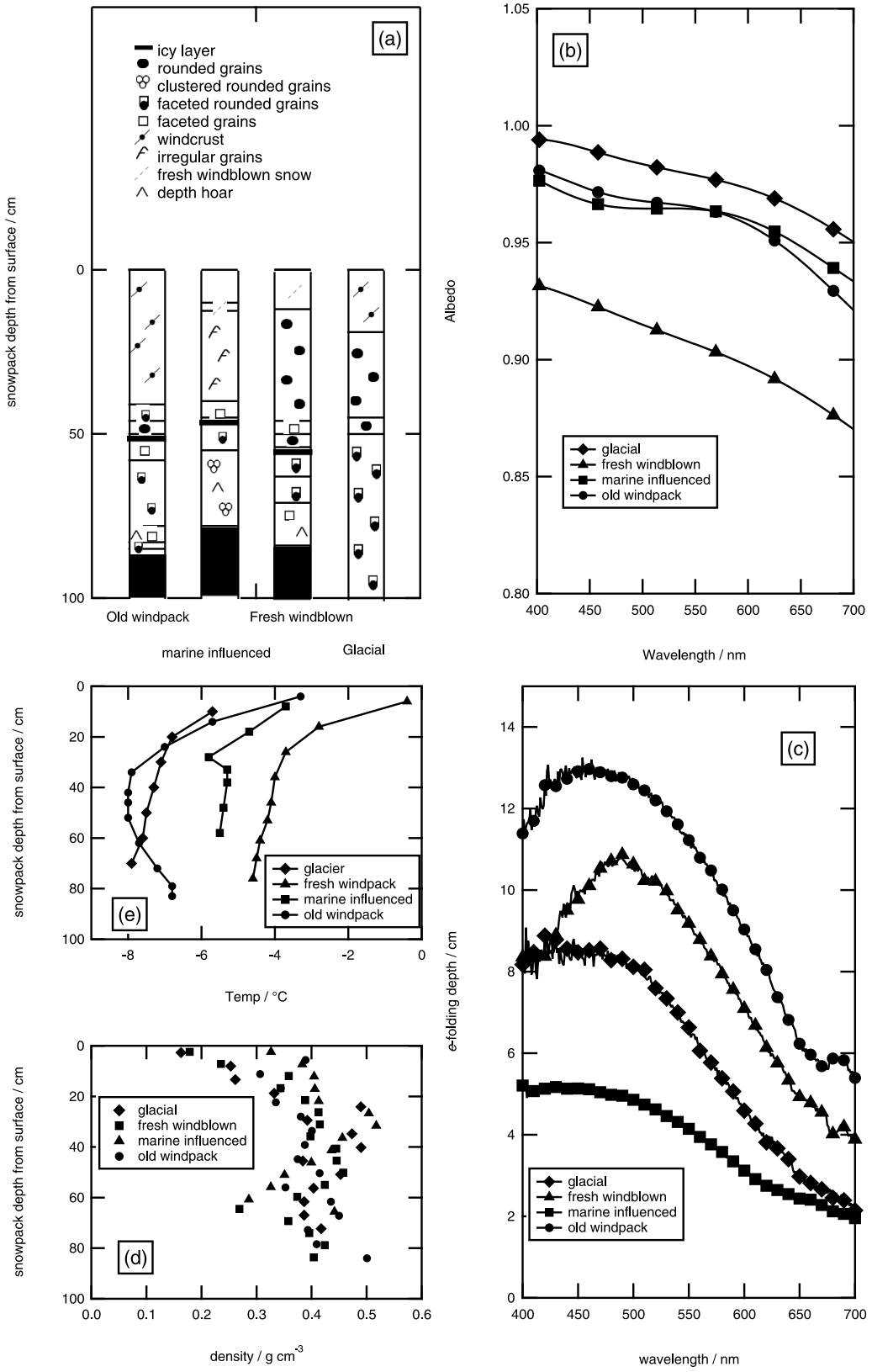

Figure 1. (a) Snowpack stratigraphy based on the notation of *Fierz et al.* [2009]. (b) Wavelength-dependent snowpack surface reflectance (albedo) (markers every 50 data points for clarity). (c) Wavelength-dependent *e*-folding depths (markers every 10 data points for clarity). (d) Snowpack density profiles. (e) Snowpack temperature profiles for each snowpack.

Table 2. Repeated Measurements of *e*-Folding Depth to Determine Uncertainty Within a Single Snowpack[a]

Site	*e*-Folding Depth[b] (cm)	Liquid Equivalent *e*-Folding Depth[b] (cm)	σ^+_{abs} ($cm^2\ kg^{-1}$)	σ_{scatt} ($m^2\ kg^{-1}$)	$\upsilon(NO_3^-)$, (10^{-10} ms^{-1}) $\theta = 60°$	$\theta = 70°$	$\theta = 80°$
1	4.2	1.7	11.5	8.5	40	19	5.7
2	4.2	1.7	11.5	8.5	40	19	5.7
3	6.9	2.8	7.5	5	60	28	8.5
4	6.2	2.5	8	5.5	56	27	8.0
5	5.4	2.2	9.5	6.5	49	23	7.0
6	4.5	1.8	11	8	42	20	6.0
7	4.3	1.7	11.5	8.5	40	19	5.7
All	5.1 ± 1.1	2.1 ± 0.4	9.8 ± 1.7	7 ± 1.5	47 ± 8.4	22 ± 3.9	6.7 ± 1.2
Relative uncertainty (%)	21	21	18	22	18	18	18

[a]The sites of the repeated measurement were 1 m apart, and an *e*-folding depth was determined from four depth measurements of irradiance at each site. The snowpack was a snowdrift, with 0.1–0.2 mm windblown crystals and a snowpack density of 0.41 g cm^{-3}. The values of transfer velocity, υ, and σ^+_{abs} and σ_{scatt} were calculated for each site.
[b]Wavelength λ = 400 nm.

snowpack types at Ny-Ålesund, but further investigation was not undertaken.

[34] The reflectivity data from the four snowpacks (Figure 1b) demonstrates that the glacial snowpack has the largest reflectivity, i.e., the least impacted by light-absorbing impurities. It is the furthest from the influence of marine, terrestrial sources or from anthropogenic input.

[35] The result of the repeated measurements of the *e*-folding depth measurements is shown in Table 2, with a relative standard deviation of 21% leading to a propagated uncertainty in depth-integrated photolysis rates of 18%. The relative standard deviation represents a measure of the uncertainty in replicate *e*-folding measurements and the natural variability of the snow.

4.2. Absorption and Scattering Cross Section Determination

[36] Values of the scattering and absorption cross-sectional coefficients, σ_{scatt} and σ^+_{abs}, determined at a wavelength of 400 nm are presented in Table 1, along with additional data describing the snow pit. The values of σ_{scatt} and σ^+_{abs} for wind packs between 0°C and −10°C are similar to previous polar determinations [*Beine et al.*, 2006] with the large absorption cross section of the fresh windblown snowpack owing to visibly obvious entrained soil and other terrestrial material from the wind events. The marine-influenced snowpack has a very large value of σ_{scatt} which is a surprise as the other snowpacks are within 1 km of the marine-influenced snowpacks, and would have been formed during similar wind events. The glacial values of σ_{scatt} and σ^+_{abs} are in keeping with permanent Arctic snowpack: the large value of σ_{scatt} is attributed to small grain size and the small value of σ^+_{abs} to the lack of impurities or anthropogenic input. Table 2 reports the derived absorption and scattering coefficients at a wavelength of 400 nm for each repeat *e*-folding depth measurement on the same snowbank. The 21% relative error in the repeatability of *e*-folding depth leads to a propagated error of 18% in σ^+_{abs} and 22% in σ_{scatt}.

[37] The absorption and scattering cross sections of the snowpack are reported at a wavelength of 400 nm and are considered invariant over the wavelength range required for nitrate and hydrogen peroxide photolysis. A wavelength of 400 nm is the shortest wavelength at which reliable snowpack surface reflectance and *e*-folding depth are reported (for both this work and previous studies). The maximum in the action spectrum of nitrate photolysis is ~302 nm [*Chu and Anastasio*, 2003]. *King and Simpson* [2001] demonstrated that for a dry Arctic snowpack, the *e*-folding depth varies by only 10% with wavelength, although variation between wavelengths of 300 nm and 400 nm may be larger for snowpacks with a nonuniform spectral absorption.

4.3. In-Snow Photolysis Rates

[38] Photolysis rate coefficients for reactions (1) and (3) were calculated for each of the four snowpacks (Table 1) at 30 solar zenith angles between 0° and 90° and at 106 separate depths within each snowpack. The photolysis rate coefficients are presented as contour plots of photolysis rate coefficient versus depth and versus solar zenith angle in Figures 2 and 3. Figures 2 and 3 can be used by other workers studying similar snowpacks to estimate photolysis rates of nitrate and hydrogen peroxide as a function of depth and solar zenith angle. The reciprocal of the photolysis rate coefficient plotted in Figures 2 and 3 are the lifetimes (with respect to photolysis) of nitrate and hydrogen peroxide at depth and solar zenith angle and may be useful for ice core studies [e.g., *Wolff et al.*, 2010].

4.4. Depth-Integrated Production Rates

[39] The depth-integrated production rates of OH radicals and NO_2 molecules were calculated for each of the four snowpacks at Ny-Ålesund. The calculated depth-integrated production rates are shown in Figure 4. The largest depth-integrated production rates of both OH radicals and NO_2 molecules are for the old wind pack. The largest depth-integrated production rates of NO_2 within the old wind pack are due to a combination of the largest *e*-folding depth and higher concentrations of nitrate compared to other snowpacks. The concentrations of H_2O_2 are assumed constant across all the snowpacks, thus the variation in depth-integrated production rates of OH radicals is due to variation in *e*-folding depth.

4.5. Snowpack Thickness

[40] Depth-integrated photolysis rates increase rapidly with snowpack depth and approach constant depth-integrated

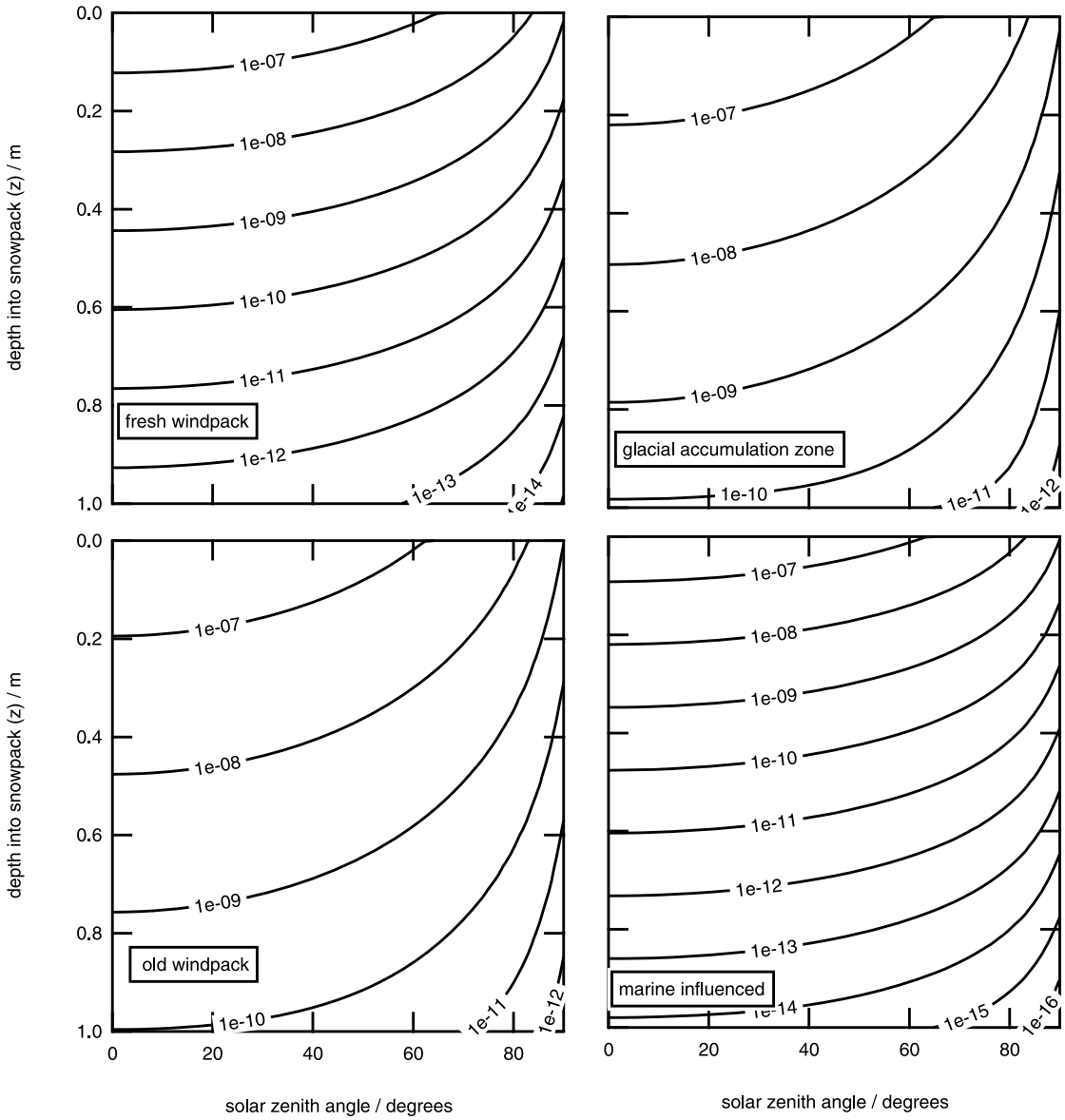

Figure 2. Photolysis rate coefficients for the photolysis of $J(NO_3^-)$ (reaction (1)) for the four snowpacks of Table 1 versus depth and solar zenith angle. Contours show equal $J(NO_3^-)$.

photolysis rates. A snow cover thickness of 10, 20, and 30 cm (~2, 4, and 6 *e*-folding depths, respectively) results in a depth-integrated production rate of nitrate photolysis within 45%, 3%, and 1% of the depth-integrated photolysis rate for an optically semi-infinite snowpack. Thus, more generally a snowpack can be considered semi-infinite if it is 4–6 *e*-folding depths thick, and a snowpack 3 *e*-folding depths thick is still within 15% of the semi-infinite value. Therefore, a thickness of 3 *e*-folding depths should be the absolute minimum snowpack thickness for approximating to a semi-infinite snowpack. Figure 5 shows a transect of snowpack thickness for the marine-influenced site, with corresponding depth-integrated photolysis rates of nitrate photolysis. Figure 5 demonstrates some of the surface variability typical of the sampling sites and the almost constant value of $\upsilon(NO_3^-)$, which is only reduced significantly for areas of very thin snowpacks. Generally a semi-infinite snowpack approximation is justified. Figure 5 also demonstrates that calculations of depth-integrated photolysis rates from a single snow pit are representative of the wider area.

[41] Below the first two centimeters in snowpack, the irradiance within the snowpack is isotropic and decreases exponentially with depth. However, in the top few centimeters, the irradiance within the snowpack is not isotropic and is sensitive to the solar zenith angle [*Warren*, 1982]. A snowpack illuminated by a large solar zenith angle has a decrease in the irradiance in the top few centimeters which decreases more rapidly with depth than an exponential, and a snowpack illuminated by a small solar zenith angle has an enhancement in irradiance in the top few centimeters [*Lee-Taylor and Madronich*, 2002]. Other workers have occasionally ignored the irradiance depth profile in the top few centimeters and approximated the decrease of irradiance as exponential. For a thin snowpack this approximation may

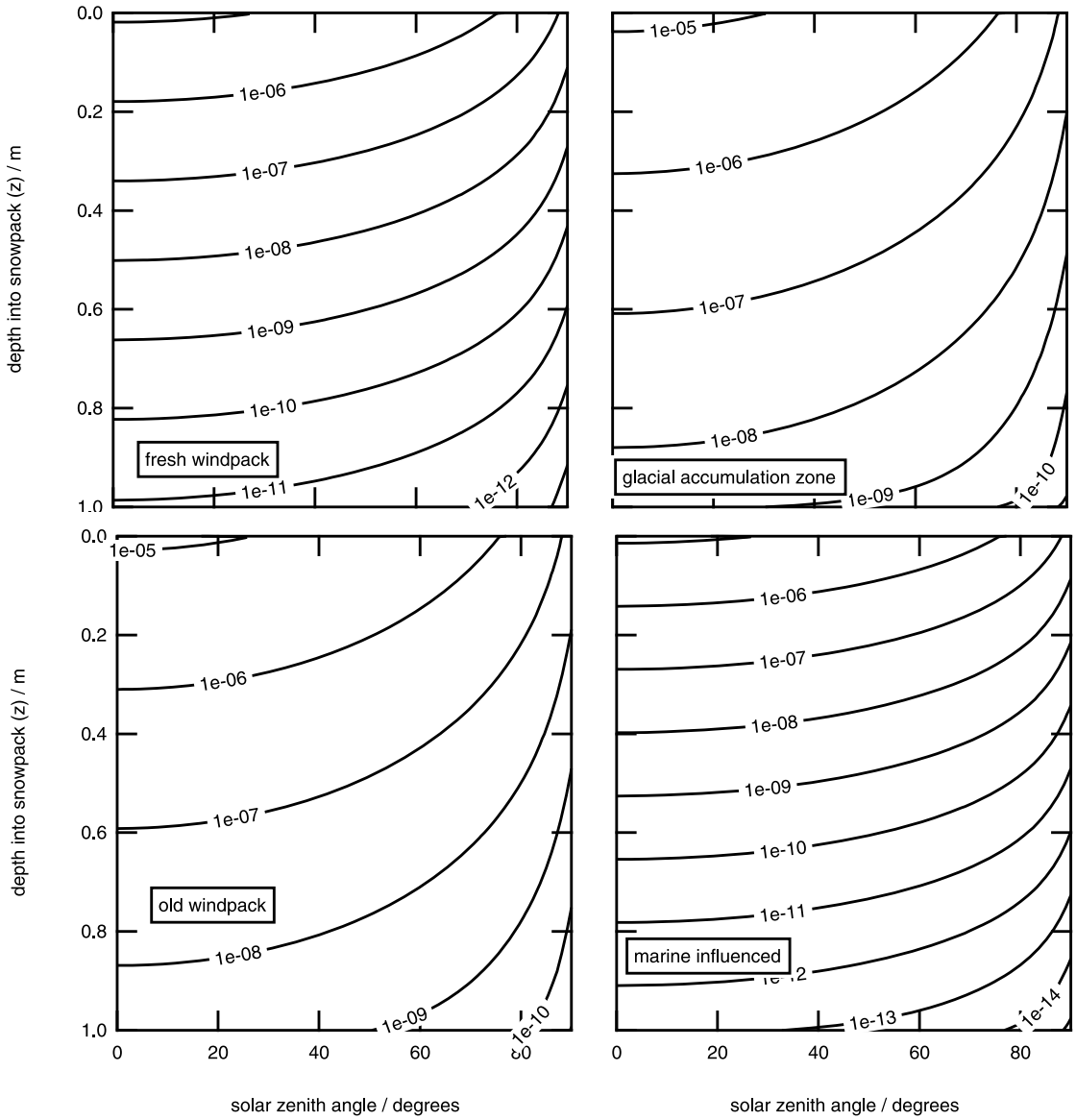

Figure 3. Photolysis rate coefficients for the photolysis of $J(H_2O_2)$ (reaction (3)) for the four snowpacks of Table 1 versus depth and solar zenith angle. Contours show equal $J(H_2O_2)$.

not be valid. The values reported here are radiative-transfer calculations that do not presume the irradiance depth profile but calculate irradiance at each depth. Depth-integrated production rates or transfer velocities should not be calculated using just surface photolysis rate coefficients and *e*-folding depths; *France et al.* [2010a] demonstrated how such assumptions can give the wrong answer for Arctic snowpacks.

5. Discussion

[42] The discussion will focus on the following five aspects of the work undertaken: (1) a comparison of *e*-folding depth measurements with other Arctic and maritime snowpacks and of modeled optical properties with other previously modeled Arctic, Antarctic and midlatitude snowpacks; (2) comparison of optical coefficients of snowpack absorption and scattering with other work; (3) calculated production rates of NO_2 and OH radicals in Ny-Ålesund snowpack, compared to measured fluxes of NO_x and an examination of the snowpack depth required for a semi-infinite snowpack depth approximation; (4) an estimation of the pseudo first-order loss rate of hydroxyl radicals in snowpack; and (5) an analysis of uncertainty in measured and calculated quantities.

5.1. Comparison of *e*-Folding Depths

[43] When comparing *e*-folding depths of snowpack, authors tend to compare the liquid equivalent *e*-folding depths, ε_{liq}, which is the *e*-folding depth normalized by the snow density [*Lee-Taylor and Madronich*, 2002; *Warren*, 1982]. Thus for the purposes of comparison, in section 5.1 (and this section alone) liquid equivalent *e*-folding depths are considered. Ny-Ålesund snowpacks have liquid equivalent *e*-folding depths of 2–4.5 cm, a little larger than

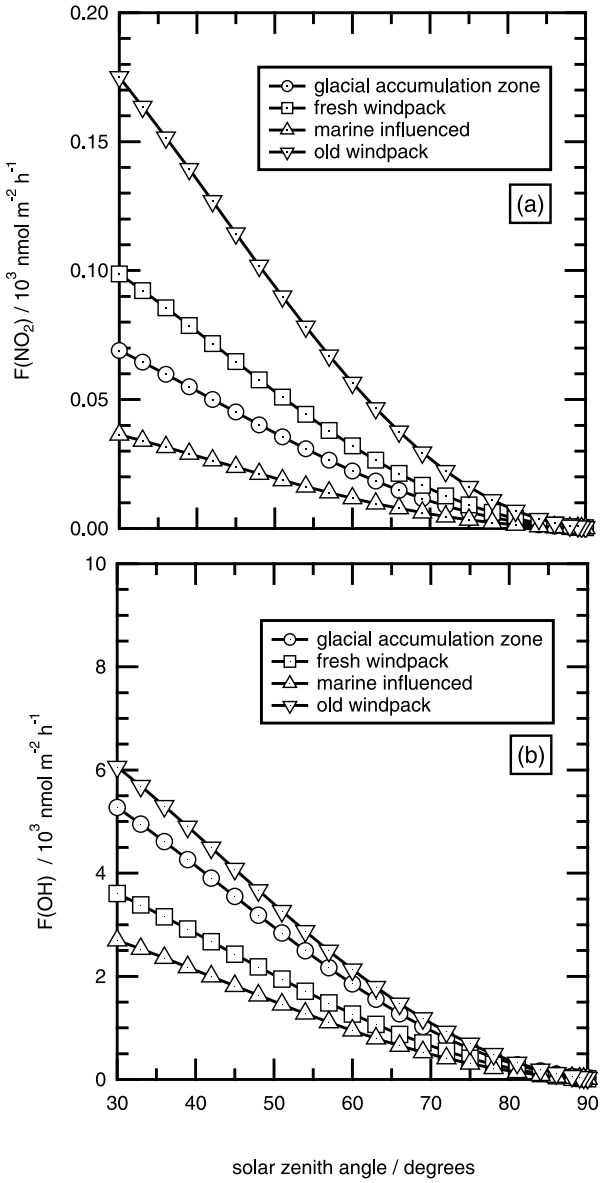

Figure 4. Calculated depth-integrated production rates (fluxes) versus solar zenith angle for clear-sky conditions for each of the four snowpacks studied near Ny-Ålesund. (a) Depth-integrated production rate (flux) of NO_2 from nitrate photolysis calculated using values of nitrate recorded in Table 1. (b) Depth-integrated production rate of OH radicals from hydrogen peroxide photolysis, assuming a concentration of 4 μmol l^{-1} of H_2O_2.

values reported for very dry, cold Arctic snowpacks, typically 2–3 cm [*King and Simpson*, 2001] but shorter than values recorded for maritime snowpacks in midlatitude regions, typically 4–7.5 cm [*Fisher et al.*, 2005]. Previous springtime liquid equivalent *e*-folding depths derived from photosynthetically active radiation (PAR) broadband measurements in Svalbard, gave values of 2.7 cm and 4 cm [*France et al.*, 2010a; *Gerland et al.*, 1999]. In previous works it has been suggested that 85% of the snowpack photochemistry occurs within the top 10 cm of a dry Arctic snowpack [*King and Simpson*, 2001] and within the top 15–60 cm of wet maritime snowpack [*Fisher et al.*, 2005]. The work presented here for Ny-Ålesund shows that 85% of the snowpack photochemistry will occur within the top 10–25 cm of the snowpack, i.e., midway between our previous studies of polar and midlatitude snowpack. The result is unsurprising as the snowpacks appeared visually to be between Arctic and Alpine types.

[44] The optical coefficients, σ_{scatt} and σ^{+}_{abs}, for the four Ny-Ålesund characteristic snowpacks are compared in Table 3, along with values of σ_{scatt} and σ^{+}_{abs} reported for other snow morphologies. The Ny-Ålesund glacial snowpack is most optically similar to the clean Antarctic snowpack [*Grenfell et al.*, 1994]. There is no local source of contaminants such as dust (other than the Mountain faces around the glaciers) or organics. The marine-influenced Ny-Ålesund snowpack has surprising optical coefficients, which the authors attribute to the proximity to the coast (within 50 m). Further experimental study is required to understand the marine-influenced snowpack. The two wind packed snows are optically similar to previously investigated coastal wind packs [*Beine et al.*, 2006], with the value of σ^{+}_{abs} an indication of the local sources of light absorbing impurities, pollution, humic material or soil and mineral dust found in the snowpack. The basal ice layer in three of the snowpacks shown in Figure 1a were too deep within the snowpack to affect the determination of the optical coefficients, i.e., the basal ice was at least 6 *e*-folding depths deeper in the snowpack and thus the snow under study was already in the semi-infinite regime.

5.2. Modeled Production Rates of NO_2 and OH at Ny-Ålesund

[45] *Amoroso et al.* [2010] detail the measured fluxes of NO_2, NO, HONO and HNO_3 chemical flux to and from the snowpack during the spring of 2006. During the period of our study the depth-integrated production rates of NO_2 in the snowpack are typically 0–30 nmol m^{-2} h^{-1} and broadly agree with magnitude of depth-integrated production rates presented here. However, *Amoroso et al.* [2010] measure extremely large dark fluxes of NO_2 and attribute these fluxes to microorganisms in the snowpack. Thus, calculated depth-integrated production rates in this work are consistent with daylight measured fluxes of *Amoroso et al.* [2010] but cannot account for the large dark fluxes of NO_2 recorded, therefore a further detailed comparison between *Amoroso et al.* [2010] and this work is not warranted.

[46] The calculated depth-integrated production rates of NO_2 due to nitrate photolysis in Ny-Ålesund snowpacks are consistent with measured values of maximum Arctic NO_x flux, i.e., maxima of 30–40 nmol m^{-2} h^{-1} at Alert for a solar zenith angle of 66° [*Beine et al.*, 2002]. The OH radical depth-integrated production rates demonstrate that the snowpack is a highly oxidizing medium in the presence of O_2 and the calculated OH radical production rates presented here may be of use for other authors determining possible sources and rates of organic chemical fluxes (such as formaldehyde or halogen activation) from the snowpack to the lower atmosphere.

[47] The variation of the depth-integrated production rates of NO_2 from nitrate photolysis between the Ny-Ålesund snowpacks (56 nmol m^{-2} s^{-1} (hard wind pack) to

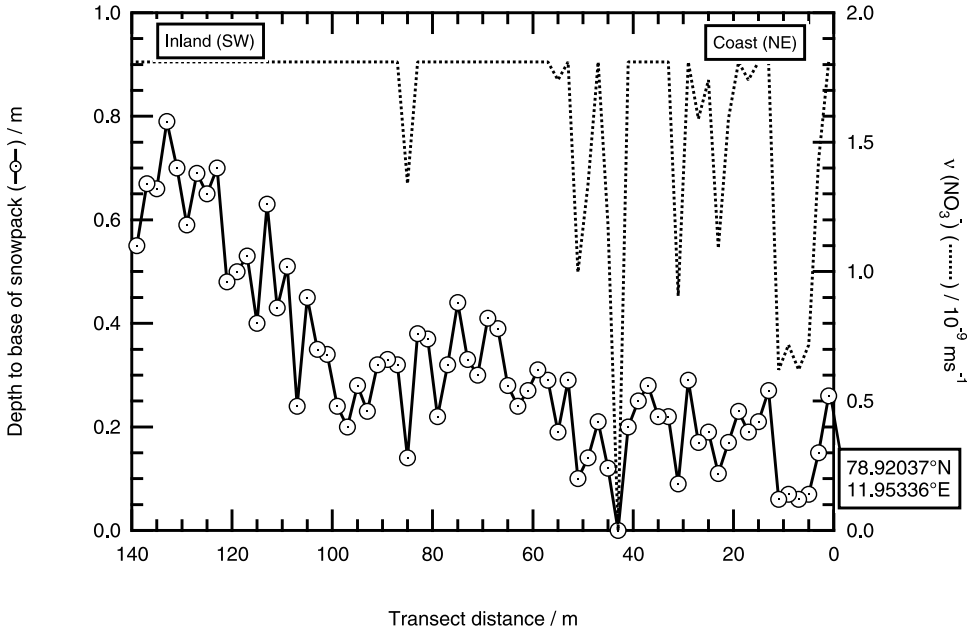

Figure 5. Transect of snow depth from the coast to inland in the Zepplinhamer region. The circular markers and solid line represent snow depth, and the dotted line with no markers is the calculated transfer velocity of nitrate for the marine-influenced snowpack for that snowpack depth. The parts of the transect where the dotted line remains flat means that with the assumption of constant physical and chemical snowpack properties, the snowpack is optically infinite and therefore is optically infinite for most of the transect.

11 nmol m^{-2} s^{-1} (marine influenced) for a solar zenith angle of 60°) is caused by a combination of differing optical properties (σ_{scatt} and σ^{+}_{abs} and differing nitrate concentration between sites (Figure 4). The very clean and highly scattering glacial accumulation zone snowpack does not produce the highest concentrations of NO_2 due to the low concentration of nitrate in the snow compared with the old wind packed snowpack, thus highlighting the importance of in-snow nitrate concentration measurements. The depth-integrated production rates of NO_2 can only be considered as maximum potential fluxes of NO_2 from the snowpack as secondary chemistry is likely to occur before all the NO_2 can exit the snowpack, e.g., the photolysis of NO_2 prior to release from the snowpack, or the snow microphysics may prevent any release at all [*Boxe et al.*, 2006]. The release of gaseous NO_2 was demonstrated to be at least partly controlled by the morphology of crystalline ice [*Boxe et al.*, 2006], and at temperatures of −8°C in controlled laboratory conditions irradiated ice doped with nitrate was shown to produce a large flux of NO_2 above the ice surface [*Boxe et al.*, 2005]. The temperatures of the snowpack at Ny-Ålesund were measured to be between −3°C and −8°C and therefore the photoproduced NO_2 can

Table 3. Modeled σ^{+}_{abs} and σ_{scatt} Coefficients Compared to Other Studies of Snowpack Optical Coefficients

Study	Snow Description	σ_{scatt} (m^2 kg^{-1})	σ^{+}_{abs} (cm^2 kg^{-1})
Grenfell and Maykut [1977]	Arctic summer dry[a]	6.4	7.3
	Arctic summer melting[a]	1.1	7.8
Grenfell et al. [1994]	Antarctic South Pole[a]	6–25	0
King and Simpson [2001]	Arctic spring windblown[a]	6–30	4–25
Beaglehole et al. [1998]	Antarctic summer coastal[a]	7–13	0.4
Fisher et al. [2005]	Midlatitude wind slab melting	1	1
	Midlatitude wind slab dry	2–5	1–2
Beine et al. [2006]	Antarctic coastal hard wind pack	1.3	4.3
	Antarctic coastal soft wind pack	6.3	24
	Antarctic coastal recent windblown	3.7	37
	Antarctic coastal precipitation	4.3	17
France et al. [2010a]	Fresh Ny-Ålesund snowpack	16.7	2.7
	Melting Ny-Ålesund snowpack	0.8	19.8
This work	Ny-Ålesund old wind pack	9.5	1.4
	Ny-Ålesund fresh wind pack	5.3	7.7
	Ny-Ålesund marine influenced	20	3.4
	Ny-Ålesund glacial	25.5	0.5

[a]Determinations of σ^{+}_{abs} and σ_{scatt} are from *Lee-Taylor and Madronich* [2002].

Table 4. Data Used in the Calculation of (and Results of) Depth-Integrated First-Order Loss Rates (Destruction Rates) of OH Radicals for Summit, Greenland, Assuming Snow Optical Properties Based on the Glacial Snowpack in the Work Presented Here[a]

Snowpack Depth (cm)	$[H_2O_2]$[b] (μmol l^{-1})	$J[H_2O_2]$[c] (10^{-5} μmol l^{-1} s^{-1})	First-Order OH Radical Loss Rate (10^3 s^{-1})
0	12	3.2	14
4	12	2.0	8.8
8	8.3	1.0	4.4
14	4.7	0.4	1.6
20	3.7	0.2	0.8

[a]Date is 27 April 2004, solar zenith angle is 59°, and $[OH]_{ss}$ is 1.4×10^6 molecule cm^{-3}. Steady state concentrations of OH radicals from *Beyersdorf et al.* [2007].
[b]Concentrations of hydrogen peroxide in the snow are from *Anastasio et al.* [2007].
[c]Calculated from values in this work.

be expected to be at least partly released as a flux from the snow surface.

[48] Hydrogen peroxide concentrations were not measured in the Ny-Ålesund snowpack, so an estimated concentration of 4 μmol l^{-1} was used. Equation (9) demonstrates that the depth-integrated production rate of OH radicals varies linearly with concentration of hydrogen peroxide. Thus it is facile to scale depth-integrated production rates of OH radicals for different concentrations of hydrogen peroxide. The difference between the depth-integrated production rates of OH radicals for the Ny-Ålesund snowpacks presented in Table 1 is approximately a factor of 2.5. *France et al.* [2010a] reviewed the literature for snowpack H_2O_2 concentrations and found that the hydrogen peroxide concentrations in Arctic snowpack can vary from 0.27 to 7.92 nmol cm^{-3} [*Hutterli et al.*, 2003], with annual average concentrations from 1.56 to 3.52 nmol cm^{-3} [*Anklin and Bales*, 1997]. A study of the surface snow concentrations at Summit, Greenland during Summer 2003 and Spring 2004 gave average H_2O_2 concentrations of 13.5 μmol l^{-1} and 11.4 μmol l^{-1}, respectively [*Anastasio et al.*, 2007]. Depth profiling of H_2O_2 concentrations at Summit show that the concentration of H_2O_2 reaches approximately 3 μmol l^{-1} by 20 cm depth into the snowpack [*Anastasio et al.*, 2007]. The variations in individual studies of H_2O_2 concentrations in snow are approximately a factor of 10 and the variation in depth-integrated production rates between Ny-Ålesund snowpacks studied here are a factor of 2.5. Thus, the variation expected in H_2O_2 concentrations is greater than the variation in depth-integrated production rates.

5.3. Estimation of First-Order Loss Rates of Hydroxyl Radicals in Snowpack

[49] *Beyersdorf et al.* [2007] inferred steady state hydroxyl radical concentrations in the surface snowpack at Summit, Greenland during campaigns in 2003–2004 from measurements of reactive volatile organic compounds that had been forced through an open chamber containing the top 40 cm of surface snow. It is not clear in the work of *Beyersdorf et al.* [2007] where in the snowpacks the reaction of OH radicals with reactive organic compounds was occurring, but *Beyersdorf et al.* [2007] produced a gas-phase pore concentration of hydroxyl radicals of approximately 1×10^6 molecules cm^{-3} within the snowpack. It is not possible to compare depth-integrated production rates of OH radicals with OH steady state concentrations in the snowpack directly. However, using the work of *Beyersdorf et al.* [2007] with the calculations presented here, it is possible to predict the first-order loss rate of OH radicals in snowpack. No information can be gained as to what the chemical loss mechanism is, and it is assumed that OH radicals are produced within the snowpack and that *Beyersdorf et al.* [2007] are not sampling atmospheric air through the snowpack. Assuming the hydroxyl radical concentration to be in steady state, then the first-order loss rate of OH radicals can be calculated from the rearrangement of

$$[OH]_{ss} = \frac{J[H_2O_2]}{\text{first-order loss rate of OH radicals}}, \qquad (11)$$

where $[OH]_{ss}$ is steady state concentration of OH radicals, J is the photolysis rate coefficient of reaction (3) and $[H_2O_2]$ is the concentration of hydrogen peroxide in the snowpack, the "first-order loss rate of OH radicals" is the loss of OH radicals within the snowpack.

[50] Equation (10) can be used to estimate first-order loss rates of OH radicals at Summit at a range of snowpack depths, assuming *Beyersdorf et al.* [2007] constant OH radical concentrations, photolysis rate coefficients from Figure 3 (glacial snowpack) and an $[H_2O_2]$ concentration for Summit snowpack from *Anastasio et al.* [2007]. All the information for the calculation of the first-order loss rates of OH radicals is in Table 4. The results of the calculated first-order loss rates of OH radicals for a range of depths (0–20 cm) in a proxy for the Summit snowpack show a range of first-order loss rates of OH radicals varies from $\sim 10^2$ s^{-1} to $\sim 10^4$ s^{-1}. The depth dependence of the first-order loss rate is probably an artifact of only having a single value of $[OH]_{ss}$, however chemical reactions that can produce a first-order loss of OH of approximately 10^3 s^{-1} are required.

5.4. Uncertainty in Measured and Calculated Quantities

[51] The variability in the measurements of reflectance and e-folding depth is considered first. Variability in repeat reflectance measurements have been previously shown to be ~10% using the single spectral radiometer method [*Fisher et al.*, 2005]. In this work, a typical 2σ uncertainty using the dual beam system is ±5%. The variability in snowpack surface reflectance is due to a combination of measurement error and natural variation of the snow surface, mainly owing to the topography. *Grenfell et al.* [1994] demonstrates that a 2° slope can give up to a 10% change in albedo, depending upon illumination angle. *Matzl and Schneebeli* [2006] show how laterally and vertically variable an apparently homogeneous snowpack can be in terms of snow specific area, thus leading to potentially imprecise radiative-transfer modeling.

[52] The results from the repeated measurement of e-folding depth are shown in Table 2. The snowpack e-folding depth was calculated seven times, each from a set of irradiance measurements at four depths. The 1σ relative uncertainty of on the e-folding depth (~20%) is much larger than expected,

and may be due to a combination of effects. The snowpack is assumed to be homogenous for all repeat measurements of *e*-folding depth, which is unlikely as the presence of buried features and icy layers cannot be discounted. Irradiances at only four depths were used, which is less than a normal experiment (where 6–10 points are used). User error through an imperfect horizontal placement of the probe by ±1 cm leads to an error of 9%–14% in the calculated *e*-folding depth [*Fisher et al.*, 2005]. The uncertainty in fiber placement far exceeds the uncertainty in spectroradiometry and therefore dominates the uncertainty in the *e*-folding depth measurement technique. The authors consider the 1σ relative error of 20% to be a maximum error. The experiment as described is the first time the uncertainty in measuring *e*-folding depth has been assessed, albeit under less than perfect conditions. It is planned to repeat this experiment during future campaigns.

6. Conclusions

[53] Field measurements of the *e*-folding depth and reflectivity of snowpacks at the Arctic atmospheric chemistry site at Ny-Ålesund, Svalbard have allowed photolysis rate coefficients for the photolysis of nitrate and hydrogen peroxide to be calculated as a function of snow type, solar zenith angle and depth. Depth integrated production rates of NO_2 and OH radical have also been calculated for four snowpacks around Ny-Ålesund during the fieldtrip. Assuming that any NO_2 photo produced in the snowpack does not undergo any secondary loss allows the depth-integrated production rate of NO_2 to be approximated to a potential snow-air flux of NO_2 owing to nitrate photolysis. The values of the calculated depth-integrated production rates broadly agrees with previous experimental flux measurements for the site [*Amoroso et al.*, 2010]. An estimation of first-order loss rates of OH radicals in Arctic snowpack varies from $\sim 10^2$ s^{-1} to $\sim 10^4$ s^{-1}. The work presented here also quantified the repeatability of *e*-folding depth measurement at ~20% which leads to a 20% error in depth-integrated production rates calculations. The work presented demonstrated that the snowpack is frequently thick enough to be considered optically infinite and that a single snow pit's optical properties may be indicative of the depth-integrated production rates of the surrounding area.

[54] **Acknowledgments.** J.L.F. wishes to thank NERC for continued support under grants NE/F010788/1, NE/F004796/1, and NER/S/A200412177. M.D.K. and J.L.F. wish to thank NERC FSF for loan 489.1205, RHUL strategy fund for a small loan, the Kirsty Brown Fund for financial support, and IPEV and CNR for logistical and in-field support. The National Center for Atmospheric Research is sponsored by the National Science Foundation. The participation of F.D. in this campaign was supported by the French Polar Institute (IPEV).

References

Abbatt, J., N. Oldridge, A. Symington, V. Chukalovskiy, R. D. McWhinney, S. Sjostedt, and R. A. Cox (2010), Release of gas-phase halogens by photolytic generation of OH in frozen halide-nitrate solutions: An active halogen formation mechanism? *J. Phys. Chem. A*, *114*, 6527–6533, doi:10.1021/jp102072t.

Amoroso, A., H. J. Beine, R. Sparapani, M. Nardino, and I. Allegrini (2006), Observation of coinciding arctic boundary layer ozone depletion and snow surface emissions of nitrous acid, *Atmos. Environ.*, *40*, 1949–1956, doi:10.1016/j.atmosenv.2005.11.027.

Amoroso, A., et al. (2010), Microorganisms in dry polar snow are involved in the exchanges of reactive nitrogen species with the atmosphere, *Environ. Sci. Technol.*, *44*, 714–719, doi:10.1021/es9027309.

Anastasio, C., and L. Chu (2009), Photochemistry of nitrous acid (HONO) and nitrous acidium ion (H_2ONO^+) in aqueous solution and ice, *Environ. Sci. Technol.*, *43*, 1108–1114, doi:10.1021/es802579a.

Anastasio, C., E. S. Galbavy, M. A. Hutterli, J. F. Burkhart, and D. K. Friel (2007), Photoformation of hydroxyl radical on snow grains at Summit, Greenland, *Atmos. Environ.*, *41*, 5110–5121, doi:10.1016/j.atmosenv.2006.12.011.

Anklin, M., and R. C. Bales (1997), Recent increase in H_2O_2 concentration at Summit, Greenland, *J. Geophys. Res.*, *102*, 19,099–19,104, doi:10.1029/97JD01485.

Askebjer, P., et al. (1997), UV and optical light transmission properties in deep ice at the South Pole, *Geophys. Res. Lett.*, *24*, 1355–1358, doi:10.1029/97GL01246.

Beaglehole, D., B. Ramanathan, and J. Rumberg (1998), The UV to IR transmittance of Antarctic snow, *J. Geophys. Res.*, *103*, 8849–8857, doi:10.1029/97JD03604.

Beine, H. J., D. A. Jaffe, F. Stordal, M. Engardt, S. Solberg, N. Schmidbauer, and K. Holmen (1997), NO_x during ozone depletion events in the Arctic troposphere at Ny-Ålesund, Svalbard, *Tellus, Ser. B*, *49*, 556–565, doi:10.1034/j.1600-0889.49.issue5.10.x.

Beine, H. J., I. Allegrini, R. Sparapani, A. Ianniello, and F. Valentini (2001), Three years of springtime trace gas and particle measurements at Ny-Ålesund, Svalbard, *Atmos. Environ.*, *35*, 3645–3658, doi:10.1016/S1352-2310(00)00529-X.

Beine, H. J., R. E. Honrath, F. Domine, W. R. Simpson, and J. D. Fuentes (2002), NO_x during background and ozone depletion periods at Alert: Fluxes above the snow surface, *J. Geophys. Res.*, *107*(D21), 4584, doi:10.1029/2002JD002082.

Beine, H. J., F. Domine, A. Ianniello, M. Nardino, I. Allegrini, K. Teinila, and R. Hillamo (2003), Fluxes of nitrates between snow surfaces and the atmosphere in the European high Arctic, *Atmos. Chem. Phys.*, *3*, 335–346, doi:10.5194/acp-3-335-2003.

Beine, H. J., A. Amoroso, F. Domine, M. D. King, M. Nardino, A. Ianniello, and J. L. France (2006), Surprisingly small HONO emissions from snow surfaces at Browning Pass, Antarctica, *Atmos. Chem. Phys.*, *6*, 2569–2580, doi:10.5194/acp-6-2569-2006.

Beine, H., A. J. Colussi, A. Amoroso, G. Esposito, M. Montagnoli, and M. R. Hoffmann (2008), HONO emissions from snow surfaces, *Environ. Res. Lett.*, *3*, 045005, doi:10.1088/1748-9326/3/4/045005.

Beyersdorf, A. J., N. J. Blake, A. L. Swanson, S. Meinardi, J. E. Dibb, S. Sjostedt, G. Huey, B. Lefer, F. S. Rowland, and D. R. Blake (2007), Hydroxyl concentration estimates in the sunlit snowpack at Summit, Greenland, *Atmos. Environ.*, *41*, 5101–5109, doi:10.1016/j.atmosenv.2006.08.058.

Bock, J., and H. W. Jacobi (2010), Development of a mechanism for nitrate photochemistry in snow, *J. Phys. Chem. A*, *114*, 1790–1796, doi:10.1021/jp909205e.

Boxe, C. S., and A. Saiz-Lopez (2008), Multiphase modeling of nitrate photochemistry in the quasi-liquid layer (QLL): Implications for NO_x release from the Arctic and coastal Antarctic snowpack, *Atmos. Chem. Phys.*, *8*, 6009–6034, doi:10.5194/acp-8-4855-2008.

Boxe, C. S., A. J. Colussi, M. R. Hoffmann, J. G. Murphy, P. J. Wooldridge, T. H. Bertram, and R. C. Cohen (2005), Photochemical production and release of gaseous NO_2 from nitrate-doped water ice, *J. Phys. Chem. A*, *109*, 8520–8525, doi:10.1021/jp0518815.

Boxe, C. S., A. J. Colussi, M. R. Hoffmann, I. M. Perez, J. G. Murphy, and R. C. Cohen (2006), Kinetics of NO and NO_2 evolution from illuminated frozen nitrate solutions, *J. Phys. Chem. A*, *110*, 3578–3583, doi:10.1021/jp055037q.

Burley, J. D., and H. S. Johnston (1992), Ionic mechanisms for heterogeneous stratospheric reactions and ultraviolet photoabsorption cross-sections for NO_2^+, HNO_3, and NO_3^- in sulfuric acid, *Geophys. Res. Lett.*, *19*, 1359–1362, doi:10.1029/92GL01115.

Chu, L., and C. Anastasio (2003), Quantum yields of hydroxyl radical and nitrogen dioxide from the photolysis of nitrate on ice, *J. Phys. Chem. A*, *107*, 9594–9602, doi:10.1021/jp0349132.

Chu, L., and C. Anastasio (2005), Formation of hydroxyl radical from the photolysis of frozen hydrogen peroxide, *J. Phys. Chem. A*, *109*, 6264–6271, doi:10.1021/jp051415f.

Cotter, E. S. N., A. E. Jones, E. W. Wolff, and S. J. B. Bauguitte (2003), What controls photochemical NO and NO_2 production from Antarctic snow? Laboratory investigation assessing the wavelength and temperature dependence, *J. Geophys. Res.*, *108*(D4), 4147, doi:10.1029/2002JD002602.

Couch, T. L., A. L. Sumner, T. M. Dassau, P. B. Shepson, and R. E. Honrath (2000), An investigation of the interaction of carbonyl com-

pounds with the snowpack, *Geophys. Res. Lett.*, *27*, 2241–2244, doi:10.1029/1999GL011288.

Dassau, T. M., et al. (2002), Investigation of the role of the snowpack on atmospheric formaldehyde chemistry at Summit, Greenland, *J. Geophys. Res.*, *107*(D19), 4394, doi:10.1029/2002JD002182.

Dibb, J. E., L. G. Huey, D. L. Slusher, and D. J. Tanner (2004), Soluble reactive nitrogen oxides at South Pole during ISCAT 2000, *Atmos. Environ.*, *38*, 5399–5409, doi:10.1016/j.atmosenv.2003.01.001.

Domine, F., and P. B. Shepson (2002), Air-snow interactions and atmospheric chemistry, *Science*, *297*, 1506–1510, doi:10.1126/science.1074610.

Domine, F., M. Albert, T. Huthwelker, H. W. Jacobi, A. A. Kokhanovsky, M. Lehning, G. Picard, and W. R. Simpson (2008), Snow physics as relevant to snow photochemistry, *Atmos. Chem. Phys.*, *8*, 171–208, doi:10.5194/acp-8-171-2008.

Dubowski, Y., A. J. Colussi, and M. R. Hoffmann (2001), Nitrogen dioxide release in the 302 nm band photolysis of spray-frozen aqueous nitrate solutions: Atmospheric implications, *J. Phys. Chem. A*, *105*, 4928–4932, doi:10.1021/jp0042009.

Dubowski, Y., A. J. Colussi, C. Boxe, and M. R. Hoffmann (2002), Monotonic increase of nitrite yields in the photolysis of nitrate in ice and water between 238 and 294 K, *J. Phys. Chem. A*, *106*, 6967–6971, doi:10.1021/jp0142942.

Duggin, M. J., and W. R. Philipson (1982), Field measurement of reflectance: Some major considerations, *Appl. Opt.*, *21*, 2833–2840, doi:10.1364/AO.21.002833.

Fierz, C., R. L. Armstrong, Y. Durand, P. Etchevers, E. Greene, D. M. McClung, K. Nishimura, P. K. Satyawali, and S. A. Sokratov (2009), The international classification for seasonal snow on the ground, *IHP-VII Tech. Doc. Hydrol. 83, IACS Contrib. 1*, U. N. Educ. Sci. Cult. Organ. Int. Hydrol. Prog., Paris.

Fisher, F. N., M. D. King, and J. Lee-Taylor (2005), Extinction of UV-visible radiation in wet midlatitude (maritime) snow: Implications for increased NO_x emission, *J. Geophys. Res.*, *110*, D21301, doi:10.1029/2005JD005963.

France, J. L. (2008), Chemical oxidation in snowpack, Ph.D. thesis, R. Holloway Univ. of London, Egham, U. K.

France, J. L., M. D. King, and J. Lee-Taylor (2007), Hydroxyl (OH) radical production rates in snowpacks from photolysis of hydrogen peroxide (H_2O_2) and nitrate (NO_3^-), *Atmos. Environ.*, *41*, 5502–5509, doi:10.1016/j.atmosenv.2007.03.056.

France, J. L., M. D. King, and J. Lee-Taylor (2010a), The importance of considering depth-resolved photochemistry in snow: A radiative-transfer study of NO_2 and OH production in Ny-Alesund snowpacks, *J. Glaciol.*, *56*, 655–663, doi:10.3189/002214310793146250.

France, J. L., M. D. King, and A. MacArthur (2010b), A photohabitable zone in the Martian snowpack? A laboratory and radiative-transfer study of dusty water-ice snow, *Icarus*, *207*, 133–139, doi:10.1016/j.icarus.2009.11.026.

France, J. L., M. D. King, F. M. Frey, J. Savarino, J. Erbland, and G. Picard (2011), Snow optical properties at Dome C, Antarctica: Implications for snow emissions and snow chemistry of reactive nitrogen, *Atmos. Chem. Phys. Discuss.*, *11*, 11,959–11,993, doi:10.5194/acpd-11-11959-2011.

George, I. J., and C. Anastasio (2007), Release of gaseous bromine from the photolysis of nitrate and hydrogen peroxide in simulated sea-salt solutions, *Atmos. Environ.*, *41*, 543–553, doi:10.1016/j.atmosenv.2006.08.022.

Gerland, S., J. G. Winther, J. B. Orbaek, G. E. Liston, N. A. Oritsland, A. Blanco, and B. Ivanov (1999), Physical and optical properties of snow covering Arctic tundra on Svalbard, *Hydrol. Processes*, *13*, 2331–2343, doi:10.1002/(SICI)1099-1085(199910)13:14/15<2331::AID-HYP855>3.0.CO;2-W.

Grannas, A. M., P. B. Shepson, and T. R. Filley (2004), Photochemistry and nature of organic matter in Arctic and Antarctic snow, *Global Biogeochem. Cycles*, *18*, GB1006, doi:10.1029/2003GB002133.

Grannas, A. M., et al. (2007), An overview of snow photochemistry: Evidence, mechanisms and impacts, *Atmos. Chem. Phys.*, *7*, 4329–4373, doi:10.5194/acp-7-4329-2007.

Grenfell, T. C., and G. A. Maykut (1977), The optical properties of ice and snow in the Arctic basin, *J. Glaciol.*, *10*, 445–463.

Grenfell, T. C., S. G. Warren, and P. C. Mullen (1994), Reflection of solar-radiation by the Antarctic snow surface at ultraviolet, visible, and near-infrared wavelengths, *J. Geophys. Res.*, *99*, 18,669–18,684, doi:10.1029/94JD01484.

Hoffer, A., A. Gelencsér, P. Guyon, G. Kiss, O. Schmid, G. P. Frank, P. Artaxo, and M. O. Andreae (2006), Optical properties of humic-like substances (HULIS) in biomass-burning aerosols, *Atmos. Chem. Phys.*, *6*, 3563–3570, doi:10.5194/acp-6-3563-2006.

Honrath, R. E., M. C. Peterson, S. Guo, J. E. Dibb, P. B. Shepson, and B. Campbell (1999), Evidence of NO_x production within or upon ice particles in the Greenland snowpack, *Geophys. Res. Lett.*, *26*, 695–698, doi:10.1029/1999GL900077.

Honrath, R. E., S. Guo, M. C. Peterson, M. P. Dziobak, J. E. Dibb, and M. A. Arsenault (2000a), Photochemical production of gas phase NO_x from ice crystal NO_3^-, *J. Geophys. Res.*, *105*, 24,183–24,190, doi:10.1029/2000JD900361.

Honrath, R. E., M. C. Peterson, M. P. Dziobak, J. E. Dibb, M. A. Arsenault, and S. A. Green (2000b), Release of NO_x from sunlight-irradiated midlatitude snow, *Geophys. Res. Lett.*, *27*, 2237–2240, doi:10.1029/1999GL011286.

Honrath, R. E., Y. Lu, M. C. Peterson, J. E. Dibb, M. A. Arsenault, N. J. Cullen, and K. Steffen (2002), Vertical fluxes of NO_x, HONO, and HNO_3 above the snowpack at Summit, Greenland, *Atmos. Environ.*, *36*, 2629–2640, doi:10.1016/S1352-2310(02)00132-2.

Hutterli, M. A., J. R. McConnell, R. C. Bales, and R. W. Stewart (2003), Sensitivity of hydrogen peroxide (H_2O_2) and formaldehyde (HCHO) preservation in snow to changing environmental conditions: Implications for ice core records, *J. Geophys. Res.*, *108*(D1), 4023, doi:10.1029/2002JD002528.

Hutterli, M. A., J. R. McConnell, G. Chen, R. C. Bales, D. D. Davis, and D. H. Lenschow (2004), Formaldehyde and hydrogen peroxide in air, snow and interstitial air at South Pole, *Atmos. Environ.*, *38*, 5439–5450, doi:10.1016/j.atmosenv.2004.06.003.

Jacobi, H. W., R. C. Bales, R. E. Honrath, M. C. Peterson, J. E. Dibb, A. L. Swanson, and M. R. Albert (2004), Reactive trace gases measured in the interstitial air of surface snow at Summit, Greenland, *Atmos. Environ.*, *38*, 1687–1697, doi:10.1016/j.atmosenv.2004.01.004.

Jones, A. E., and E. W. Wolff (2003), An analysis of the oxidation potential of the South Pole boundary layer and the influence of stratospheric ozone depletion, *J. Geophys. Res.*, *108*(D18), 4565, doi:10.1029/2003JD003379.

Jones, A. E., R. Weller, E. W. Wolff, and H. W. Jacobi (2000), Speciation and rate of photochemical NO and NO_2 production in Antarctic snow, *Geophys. Res. Lett.*, *27*, 345–348, doi:10.1029/1999GL010885.

Jones, A. E., R. Weller, P. S. Anderson, H. W. Jacobi, E. W. Wolff, O. Schrems, and H. Miller (2001), Measurements of NO_x emissions from the Antarctic snowpack, *Geophys. Res. Lett.*, *28*, 1499–1502, doi:10.1029/2000GL011956.

King, M. D., and W. R. Simpson (2001), Extinction of UV radiation in Arctic snow at Alert, Canada (82°N), *J. Geophys. Res.*, *106*, 12,499–12,507, doi:10.1029/2001JD900006.

King, M. D., J. L. France, F. N. Fisher, and H. J. Beine (2005), Measurement and modelling of UV radiation penetration and photolysis rates of nitrate and hydrogen peroxide in Antarctic sea ice: An estimate of the production rate of hydroxyl radicals in first-year sea ice, *J. Photochem. Photobiol. Chem.*, *176*, 39–49, doi:10.1016/j.jphotochem.2005.08.032.

Lee-Taylor, J., and S. Madronich (2002), Calculation of actinic fluxes with a coupled atmosphere-snow radiative transfer model, *J. Geophys. Res.*, *107*(D24), 4796, doi:10.1029/2002JD002084.

Mack, J., and J. R. Bolton (1999), Photochemistry of nitrite and nitrate in aqueous solution: A review, *J. Photochem. Photobiol. Chem.*, *128*, 1–13, doi:10.1016/S1010-6030(99)00155-0.

Matthew, B. M., I. George, and C. Anastasio (2003), Hydroperoxyl radical (HO_2) oxidizes dibromide radical anion (Br_2^-) to bromine (Br_2) in aqueous solution: Implications for the formation of Br_2 in the marine boundary layer, *Geophys. Res. Lett.*, *30*(24), 2297, doi:10.1029/2003GL018572.

Matzl, M., and M. Schneebeli (2006), Measuring specific surface area of snow by near-infrared photography, *J. Glaciol.*, *52*, 558–564, doi:10.3189/172756506781828412.

Mauldin, R. L., et al. (2001), Measurements of OH, H_2SO_4, and MSA at the South Pole during ISCAT, *Geophys. Res. Lett.*, *28*, 3629–3632, doi:10.1029/2000GL012711.

McPeters, R. D., A. J. Krueger, P. K. Bhartia, and J. R. Herman (1998), Earth Probe Total Ozone Mapping Spectrometer (TOMS) data products user's guide, *NASA Tech. Publ. 1998-206895*, Goddard Space Flight Cent., Greenbelt, Md.

Perovich, D. K., and J. W. Govoni (1991), Absorption co-efficients of ice from 250 nm to 400 nm, *Geophys. Res. Lett.*, *18*, 1233–1235, doi:10.1029/91GL01642.

Phillips, G. J., and W. R. Simpson (2005), Verification of snowpack radiation transfer models using actinometry, *J. Geophys. Res.*, *110*(D8), D08306, doi:10.1029/2004JD005552.

Piot, M., and R. von Glasow (2008), The potential importance of frost flowers, recycling on snow, and open leads for ozone depletion events, *Atmos. Chem. Phys.*, *8*, 2437–2467, doi:10.5194/acp-8-2437-2008.

Pope, R. M., and E. S. Fry (1997), Absorption spectrum (380–700 nm) of pure water. 2. Integrating cavity measurements, *Appl. Opt.*, *36*, 8710–8723, doi:10.1364/AO.36.008710.

Shepson, P. B., A. P. Sirju, J. F. Hopper, L. A. Barrie, V. Young, H. Niki, and H. Dryfhout (1996), Sources and sinks of carbonyl compounds in the Arctic Ocean boundary layer: Polar ice floe experiment, *J. Geophys. Res.*, *101*, 21,081–21,089, doi:10.1029/96JD02032.

Simpson, W. R., M. D. King, H. J. Beine, R. E. Honrath, and X. L. Zhou (2002), Radiation-transfer modeling of snow-pack photochemical processes during ALERT 2000, *Atmos. Environ.*, *36*, 2663–2670, doi:10.1016/S1352-2310(02)00124-3.

Stamnes, K., S. C. Tsay, W. Wiscombe, and K. Jayaweera (1988), Numerically stable algorithm for discrete-ordinate-method radiative-transfer in multiple-scattering and emitting layered media, *Appl. Opt.*, *27*, 2502–2509, doi:10.1364/AO.27.002502.

Wang, Y. H., Y. Choi, T. Zeng, D. Davis, M. Buhr, L. G. Huey, and W. Neff (2008), Assessing the photochemical impact of snow NO_x emissions over Antarctica during ANTCI 2003, *Atmos. Environ.*, *42*, 2849–2863, doi:10.1016/j.atmosenv.2007.07.062.

Warren, S. G. (1982), Optical properties of snow, *Rev. Geophys.*, *20*, 67–89, doi:10.1029/RG020i001p00067.

Warren, S. G., and R. E. Brandt (2008), Optical constants of ice from the ultraviolet to the microwave: A revised compilation, *J. Geophys. Res.*, *113*, D14220, doi:10.1029/2007JD009744.

Warren, S. G., R. E. Brandt, and T. C. Grenfell (2006), Visible and near-ultraviolet absorption spectrum of ice from transmission of solar radiation into snow, *Appl. Opt.*, *45*, 5320–5334, doi:10.1364/AO.45.005320.

Wiscombe, W. J., and S. G. Warren (1980), A model for the spectral albedo of snow. 1. Pure snow, *J. Atmos. Sci.*, *37*, 2712–2733, doi:10.1175/1520-0469(1980)037<2712:AMFTSA>2.0.CO;2.

Wolff, E. W., et al. (2010), Changes in environment over the last 800,000 years from chemical analysis of the EPICA Dome C ice core, *Quat. Sci. Rev.*, *29*, 285–295, doi:10.1016/j.quascirev.2009.06.013.

Yang, J., R. E. Honrath, M. C. Peterson, J. E. Dibb, A. L. Sumner, P. B. Shepson, M. Frey, H. W. Jacobi, A. Swanson, and N. Blake (2002), Impacts of snowpack emissions on deduced levels of OH and peroxy radicals at Summit, Greenland, *Atmos. Environ.*, *36*, 2523–2534, doi:10.1016/S1352-2310(02)00128-0.

H. J. Beine, Air Quality Research Centre, University of California, 1 Shields Ave., Davis, CA 95616-8627, USA.

F. Domine, Laboratoire de Glaciologie et Géophysique de l'Environnement, CNRS, BP 96, F-38402 St. Martin D'Heres CEDEX, France.

J. L. France and M. D. King, Department of Earth Sciences, Royal Holloway University of London, Egham Hill, Egham TW20 0EX, UK. (m.king@es.rhul.ac.uk)

A. Ianniello, Consiglio Nazionale delle Ricerche-IIA, Via Salaria Km 29, 3, I-00016 Monterotondo Scalo, Rome, Italy.

J. Lee-Taylor, Atmospheric Chemistry Division, National Center for Atmospheric Research, PO Box 3000, Boulder, CO 80307, USA.

A. MacArthur, Grant Institute, University of Edinburgh, West Mains Road, Edinburgh EH9 3JW, UK.